

THE EFFECT OF THE PROTON AND NEUTRON AS PROBE FOR THE NUCLEAR FUSION REACTIONS AT NEAR-BARRIER ENERGIES[†]

✉M.A. Khuadher*, ✉F.A. Majeed[§]

Department of Physics, College of Education for Pure Sciences, University of Babylon, Iraq

**Corresponding Author e-mail: muntazer.ahmed.kh.1998@gmail.com*

§e-mail: fmajeed@uobabylon.edu.iq

Received May 5; revised June 15, 2023; accepted June 15, 2023

In this study, quantum mechanical calculations and a semi-classical approach were used to determine fusion the probability (P_{fus}), fusion barrier distribution (D_{fus}), and fusion cross section (σ_{fus}) for the systems $^{28}\text{Si} + ^{90}\text{Zr}$, $^{28}\text{Si} + ^{92}\text{Zr}$, $^{28}\text{Si} + ^{94}\text{Zr}$, $^{41}\text{K} + ^{28}\text{Si}$, and $^{45}\text{K} + ^{28}\text{Si}$. The semi-classical approach involved the use of the Wentzel–Kramers–Brillouin (WKB) approximation to describe the relative motion between the projectile and target nuclei, and the Continuum Discretized Coupled Channel (CDCC) method of Alder–Winther (AW) to describe the intrinsic motion of the nuclei. The results showed that the consideration of the coupling-channel calculations for quantum mechanics and a semi-classical approach, and its impact on P_{fus} , D_{fus} , and σ_{fus} for the studied systems involving one neutron or one proton transfer reactions are very important to be considered specifically around and below the Coulomb barrier. The results were compared with the measured data and found in reasonable agreement.

Keywords: Breakup channel, Elastic channel, Nuclear fusion, Neutron transfer, Proton transfer

PACS: 34. 85. +x, 24.10.-i, 25.70.Jj

1. INTRODUCTION

Nature displays one of its most impressive processes through the fusion of atomic nuclei. When the two nuclei merge with adequate kinetic energy they are capable of overcoming their electrostatic attraction to one another and producing a new nucleus with a charge and baryon number equal to the total of the original nuclei. The method of fusion depends on the amount of available kinetic energy, and The Coulomb barrier can be crossed or penetrated using quantum mechanical tunneling [1]. In the creation of elements, the involvement of nuclei with a high neutron content is critical, whether it occurs naturally in astronomical events or experiments carried out on Earth. The production of heavy and superheavy nuclei using the neutron-richest projectiles and targets possible is favored by experimental and theoretical data [2-3]. Neutron-rich nuclei fusion is thought to create heat that can cause an X-ray superburst in an accreting neutron star, according to a hypothesis [4]. Where systems rich in neutrons are a rich material for research and exploration. In the investigation of the fusion of $^{58}\text{Ni} + ^{64}\text{Ni}$ at $Q+2n = 3.9\text{MeV}$, Beckerman et al first noticed the impact of Positive Q-value Neutron Transfer (PQNT) [5] channels on near-barrier fusion cross sections. They directly compared the fusion excitation functions of $^{58,64}\text{Ni} + ^{58,64}\text{Ni}$ in an experiment, with the symbol “+” notation representing the absorption of neutrons from the target nuclei [6]. According to Broglia et al, the sub-barrier enhancement of fusion observed in $^{58}\text{Ni} + ^{64}\text{Ni}$ is due to a kinematic effect caused by the transfer of two neutrons during the fusion process, which reduces the neutron transfer cross-section [7] In some cases, the strength of the PQNT channels correlates strongly with the sub-barrier improvement of fusion[8]. In comparison to $^{32}\text{S}+^{90}\text{Zr}$, the sub-barrier cross sections for $^{32}\text{S}+^{96}\text{Zr}$ are significantly greater. A coupled-channels calculation that considers the inelastic excitations can explain the sub-barrier improvement in $^{32}\text{S}+^{90}\text{Zr}$ only. Nonetheless, the unaccounted-for part of $^{32}\text{S}+^{96}\text{Zr}$ is thought to be connected to intermediate multi-neutron transfers with a positive-Q value. According to the similarities between $^{40}\text{Ca}+^{96}\text{Zr}$ and $^{32}\text{S}+^{96}\text{Zr}$, couplings to positive-Q-value multi-neutron transfer channels may have improved sub-barrier fusion [9]. It is noteworthy that the fusion cross sections for the $^{24}\text{O}+^{58}\text{Ni}$ and $^{40}\text{Ca}+^{96}\text{Zr}$ systems display different patterns in the vicinity of the barrier due to the contribution of the one-neutron transfer channel. While this channel has negligible impact on the $^{40}\text{Ca}+^{96}\text{Zr}$ reaction, it plays a significant role in the $^{24}\text{O}+^{58}\text{Ni}$ reaction. This discrepancy can be attributed to the distinct one-neutron transfer channel's Q-values, which are $Q_{1n} = 5.29\text{ MeV}$ and $Q_{1n} = 0.508\text{ MeV}$ for $^{24}\text{O}+^{58}\text{Ni}$ and $^{40}\text{Ca}+^{96}\text{Zr}$, respectively [10]. A density-constrained Time-Dependent Hartree-Fock (TDHF) [11] approach to fusion theory predicts increased fusion in the $^{24}\text{O} + ^{16}\text{O}$ system relative to the $^{16}\text{O} + ^{16}\text{O}$ system due to neutron transfer altering the potential and reducing the barrier. However, the fusion neutron-rich symmetric systems such as $^{24}\text{O} + ^{24}\text{O}$ is suppressed by a repulsive Pauli potential caused by the overlapping neutron-rich tails. [2] With the addition of one neutron to ^{18}O , the experimental fusion cross-section above the barrier rises by 37%, which is a remarkable outcome. The researcher's analysis showed that the rise in the fusion cross-section for ^{19}O is not the outcome of an odd-even effect, and the improvement in the fusion cross-section of ^{19}O is not a standard excitation.[4] Thought it was because of unpaired neutrons [12]. When comparing neutron-rich and non-neutron-rich systems, the N/Z ratio at the neck region is higher in the former. This increase in the N/Z ratio leads to a decrease in the Coulomb barrier, which enhances the fusion cross-sections in neutron-rich systems[13]. Between interacting nuclei, neutron transfers can form a neck region of nuclear matter that encourages fusion. Once the nuclei are sufficiently close to one another to interact noticeably, or if positive Q-values for neutron transfers, neutron pick-up events

[†] Cite as: M.A. Khuadher, F.A. Majeed, East Eur. J. Phys. 3, 178 (2023), <https://doi.org/10.26565/2312-4334-2023-3-14>

© M.A. Khuadher, F.A. Majeed, 2023

take place [14]. Broad distributions of experimental fusion cross-sections are produced by sequential neutron transfers. Neutron flow may result from the development of a neck between the projectile and target as a result of a collision with a finite Q-value [15]. This could act as fusion's "doorway state". This intermediate state lowers the barrier and makes the fusion process easier at energies below the barrier, significantly increasing fusion cross-sections. An increase in sub-barrier fusion cross-sections has already been shown by experimental findings using (PQNT) [16-17]. It has been proposed by Zagrebaev that the transfer of particles with negative Q values does not increase fusion at energies near or below the barrier [18]. Based on a quantum diffusion approach, Sargsyan and co-workers suggested it if the deformation strength of the nuclei involved in neutron transfer does not change or decrease, neutron transfer channels have little impact on fusion dynamics. Consequently, in some instances, transfer channels may not lead to significant sub-barrier fusion enhancements despite (PQNT) [19]. A universal fusion function approach was used by researchers to analyze the effects of (PQNT) on the fusion process in various systems. They found that significant deformation of the interacting nuclei following neutron transfer is crucial for strong sub-barrier fusion enhancement due to the (PQNT). In contrast, if the deformation of the nuclei is minimal or decreases after neutron transfer, these channels have little effect on the fusion cross-sections [20].

Majeed et al. conducted an extensive study of the nuclear fusion process around and below the Coulomb barrier, the study included weakly bound nuclei ${}^6\text{Li} + {}^{64}\text{Ni}$, ${}^{11}\text{B} + {}^{159}\text{Tb}$, and ${}^{12}\text{C} + {}^9\text{Be}$ using the semi-classical approach and full quantum mechanics, and they reached the results that the inclusion of the breakup channel is very important, To describe σ_{fus} and D_{fus} where results improve around and below the Coulomb barrier for light projectiles [21]. To verify the results, different systems ${}^6\text{Li} + {}^{209}\text{Bi}$, ${}^7\text{Li} + {}^{209}\text{Bi}$, and ${}^9\text{Be} + {}^{208}\text{Pb}$ were studied. Similar results were reached in the previous research [22], by Fouad A. Majeed and Yousif A. Abdul-Hussien conducted a study on systems ${}^{17}\text{F} + {}^{208}\text{Pb}$ and ${}^{15}\text{C} + {}^{232}\text{Th}$ and found that the couple-channel effect between the elastic and continuous channel is very necessary for the calculations of σ_{fus} and D_{fus} where the results improved below and around the Coulomb barrier are very significant about the full quantum mechanics approach, [23]. To confirm the results they reached, they did another study of the systems ${}^6\text{He} + {}^{238}\text{U}$ and ${}^8\text{He} + {}^{197}\text{Au}$ that improved the calculations around and below the Coulomb barrier [23].

The present study aims to investigate the effect of neutron or proton transfer and the impact of coupling between the elastic and breakup channels on the calculations of σ_{fus} , D_{fus} , and P_{fus} , for the systems ${}^{28}\text{Si} + {}^{90}\text{Zr}$, ${}^{28}\text{Si} + {}^{92}\text{Zr}$, ${}^{28}\text{Si} + {}^{94}\text{Zr}$, ${}^{41}\text{K} + {}^{28}\text{Si}$, and ${}^{45}\text{K} + {}^{28}\text{Si}$. And compare the results with the related experimental data.

2. THE SEMICLASSICAL THEORY

2.1 No-Coupling or One-Channel Description

One-dimensional potential models have been utilized to evaluate the fusion Cross-section by employing the semiclassical theory. This model assumes that the degree of freedom of the colliding heavy ions can only be described by their relative motion [25, 26]. The Schrödinger equation is central to the semi-classical theory, which takes into account the energy and angular momentum of the system as well as the energy of the potential of the radial component of relative motion. Quantum tunneling is also considered in this theory. As a result, the semi-classical theory provides a comprehensive framework for understanding the behavior of quantum systems. cross-section of the fusion can be evaluated by implementing the semi-classical theory within the one-dimensional potential model [22].

$$\left(\frac{-\hbar^2\nabla^2}{2\mu} + V(r) - E\right) \psi(r) = 0. \quad (1)$$

In this context, the system's potential is denoted by $V(r)$, while μ represents the reduced mass of the system. To determine the wave-functions described in equation 1, one can utilize the time-dependent Schrodinger equations. To accomplish this, one can propose a particle trajectory based on Rutherford's usual trajectory. And include the real component of both the Coulomb potential and the centrifugal potential, which is expressed in [26]. This methodology allows for the estimation of said wave-functions.

$$V(r) = V_C(r) + V_N(r) + V_\ell(r). \quad (2)$$

To consider profound absorption in the classically prohibited elastic channel scattering coupled-channel calculations, including the imaginary part of nuclear potential., which is complex, is essential [26].

$$V_N(r) = U_N(r) - iW(r). \quad (3)$$

Researchers have employed the wave expansion technique to investigate the considerable absorption resulting from the interference of (ℓ)waves, which originates from both the actual and imaginary components of the nuclear potential. Previous studies, as per the semi-classical theory, have demonstrated that fusion arises when two nuclei approach each other and pass through the potential barrier to enter the inner region. In this scenario, the WKB method can be utilized to determine the probability of penetration below the barrier. These findings have been documented in multiple sources, including references [25, 27, 28, 29, 30].

$$P_{fus}^{WKB}(\ell, E) = \left[1 + e^{\left(2 \int_{r_b}^{r_a} K_\ell(r) dr \right)} \right]^{-1} \quad (4)$$

Eqn. 4 can be expressed as where the local wave-function number is ℓ (r), limits, r_a^ℓ and r_b^ℓ are as defined by places of turning to the classical trajectory.

$$P_{fus}^{WKB}(\ell, E) = \left[1 + e^{\frac{2\pi}{\hbar\Omega_l}(V_b(\ell)-E)} \right]^{-1} \quad (4)$$

Given that the fusion barrier can be adjusted using a parabolic function, the Hill-Wheeler formula [26] can be employed to depict the likelihood of penetration.

$$P_{fus}^{WH}(\ell, E) = \left[1 + e^{\frac{2\pi}{\hbar\Omega_l}(E-V_b(\ell))} \right]^{-1} \quad (5)$$

The fusion barrier cross-section can be calculated using equations [28,31] by employing the (WKB) approximation, where Ω_l and $V_b(l)$ represent the curvature and height parameters of the barrier, respectively. The energy from the projectile bombing the target is indicated by E .

$$\sigma_F(E) = \frac{\pi}{k^2} \sum (2\ell + 1) P_{fus}^{WKB}(\ell, E) \quad (7)$$

$$P_{fus}^\gamma(\ell, E) = \frac{4k}{E} \int |u_{\gamma\ell}(k_\gamma, r)|^2 W_{fus}^\gamma(r) \quad (8)$$

The radial component of the wave-function for the ℓ partial wave in the γ -channel is denoted by $u_{\gamma\ell}(k_\gamma, r)$, while the potential imaginary part is represented by $W_{fus}^\gamma(r)$.

2.2. The Coupled Channels Formalism

To depict the collision, we're using the projectile-to-target separation vector \vec{r} and the projectile's appropriate intrinsic degrees of freedom ζ . To simplify, we do not consider the internal arrangement of the target. The Hamiltonian can be expressed as [32].

$$H = H_0(\xi) + V(\vec{r}, \xi) \quad (9)$$

In this study, we ignore the nuclear coupling and focus solely on the interaction between the projectile and the target, which is represented by the term $V(\vec{r}, \xi)$ in the intrinsic Hamiltonian of the projectile denoted as $H_0(\xi)$. We limit our theoretical comparison to the Coulomb dipole term. The equation [32] provides the eigenvectors of $H_0(\xi)$.

$$H_0|\varphi_\beta\rangle = \varepsilon_\beta|\varphi_\beta\rangle \quad (10)$$

The energy of internal motion is denoted by ε_β , and the Alder and Winther (AW) [33] approach involves two main steps. Firstly, classical mechanics is used to model the time growth of variable \vec{r} , where the resulting trajectory is influenced by angular momentum ℓ and collision energy E . In the original version of AW, a symmetrized Rutherford trajectory was utilized. However, in our case, the trajectory is determined by solving classical equations of motion with the potential $V(\vec{r}) = \langle \varphi_0 | V(\vec{r}, \xi) \varphi_0 \rangle$, where $|\varphi_{\beta 0}\rangle$ represents the ground state of the projectile. This transforms the coupling interaction into a time-dependent interaction in the ξ -space, given by $V_\ell(\xi, t) \equiv V(\vec{r}_\ell(t), \xi)$. The second step involves treating the dynamics in the intrinsic space as a problem in time-dependent quantum mechanics. This is achieved by expanding the wave function based on intrinsic eigenstates [33].

$$\psi(\xi, t) = \sum_\beta a_\beta(\ell, t) \varphi_\beta(\xi) e^{-\frac{i\varepsilon_\beta t}{\hbar}} \quad (11)$$

By plugging this spread into the Schrödinger equation for the wave function $\psi(\xi, t)$, we arrive at the AW equations as described in reference [28].

$$i\hbar\dot{a}_\beta(\ell, t) = \sum_\alpha a_\alpha(\ell, t) \langle \varphi_\beta | V_\ell(\xi, t) | \varphi_\alpha \rangle e^{-\frac{i(\varepsilon_\beta - \varepsilon_\alpha)t}{\hbar}} \quad (12)$$

To solve these equations, the initial conditions used were $a_\beta(\ell, t \rightarrow -\infty) = \delta_{\beta 0}$. This signifies that the projectile was in its ground state before the collision ($t \rightarrow -\infty$). The resulting population of the channel after the collision corresponds to a specific angular momentum ℓ : $P_\ell^\beta = |a_\beta(\ell, t \rightarrow +\infty)|^2$, the cross-section of the angle-integrated [33]

$$\sigma_\beta = \frac{\pi}{k^2} \sum_\ell (2\ell + 1) P_\ell^{(\beta)} \quad (13)$$

To apply this technique to fusion reactions, we begin by utilizing quantum mechanics to compute the fusion cross section in a coupled-channel scenario. To simplify the process, we assume that all channels are bound and have no spins.

The total fusion cross-section can be obtained by adding up the contributions from each channel. By conducting partial-wave expansions, we arrive at the following equation as shown in reference [34].

$$\sigma_{F\&} = \sum_{\beta} \left[\frac{\pi}{k^2} \sum_{\ell} (2\ell + 1) P_{\ell}^F(\beta) \right]. \tag{14}$$

$$P_{\ell}^F(\beta) = \frac{4k}{E} \int W_{\beta}^F(r) |u_{\beta\ell}(k_{\beta}, r)|^2. \tag{15}$$

The optical potentials of the imaginary part connected to fusion in the channel ($u_{\beta\ell}(k_{\beta}, r)$) above have an absolute value of (W_{β}^F) and the radial wave function for the ℓ th partial wave is (β) in the equation above.

One possible way to estimate the likelihood of fusion occurring is by using the following approximation:

$$P_{\ell}^{(\beta)} \cong \tau_{\ell} |a_{\beta}(\ell, t_{ca})|^2. \tag{16}$$

Let τ_{ℓ} denote the transmission factor through the barrier, and $|a_{\beta}(\ell, t_{ca})|^2$ be the probability of finding the system in the channel β at the point of closest approach (t_{ca}). [35-36]

3. Distribution of Fusion Barrier

$$D_{fus}(E) = \frac{d^2 F(E)}{dE^2}. \tag{17}$$

Accurately determining the distribution of the fusion barrier parameter D_{fus} is crucial, as it is highly sensitive and has been defined in previous research [29, 31]. The function denoted as $F(E)$ represents the distribution of fusion barriers and is defined as follows:

$$F(E) = E\sigma_{fus}(E) \tag{18}$$

Considerable progress has been made in comprehending the fusion reaction by establishing the reaction fusion barrier distribution through experimentation. To determine the uncertainties in numerical fusion barrier calculations, it is possible to refer to the reaction [37, 38].

$$D_{fus}(E) \cong \frac{F(E+\Delta E)+F(E-\Delta E)-2F(E)}{\Delta E^2} \tag{19}$$

In this case, the cross-sectional data were measured at various excitation energy points, with an interval of ΔE . To determine the statistical error, the relation [29] was utilized.

$$\delta D_{fus}^{stat}(E) \approx \frac{[[\delta F(E+\Delta E)]^2 + [\delta F(E-\Delta E)]^2 + 4[\delta F(E)]^2]^{\frac{1}{2}}}{\Delta E^2} \tag{20}$$

The uncertainty in the product of ($E\sigma_f$) for each collision energy, denoted by $\delta F(E)$, is given as [29].

$$\delta D_{fus}^{stat}(E) \cong \frac{\sqrt{6}\delta F(E)}{[\Delta E]^2} \tag{21}$$

4. RESULTS AND DISCUSSION

This section presents the theoretical calculations of the fusion reaction σ_{fus} , the fusion barrier distribution D_{fus} and the fusion probability P_{fus} . These calculations were obtained using the semi-classical theory with a Continuum Discretized Coupled Channel (CDCC) [39] approach to study the effect of calculating the coupling between elastic channels and breakup channels on fusion processes. The calculations were performed using the Sequential Complete Fusion SCF [40] code for semi-classical comparisons, while the quantum mechanical calculations were performed using the CC code for the systems, $^{28}\text{Si} + ^{90}\text{Zr}$, $^{28}\text{Si} + ^{92}\text{Zr}$, $^{28}\text{Si} + ^{94}\text{Zr}$, $^{41}\text{K} + ^{28}\text{Si}$, and $^{45}\text{K} + ^{28}\text{Si}$. Table 1 presents the parameters for the Akyüz-Winther potential, with a coulomb barrier.

Table 1. The Coulomb barrier height V_b and The Akyüz-Winther potential parameters

System	Real part				Imaginary part				V_b
	V_o	r_o	a_o	w_o	r_i	a_i	L_{max}	L_{min}	
28Si+90Zr	-146.1	1.055	0.800	-27.7	1.007	0.736	63	0	73.66
28Si+92Zr	-60.1	1.210	0.850	-14.4	1.007	0.736	31	0	72.15
28Si+94Zr	-140	1.100	0.800	-27.0	1.008	0.735	57	0	71.44
41K+28Si	-46.0	1.212	0.655	-15.3	0.983	0.750	46	0	37.48
45K+28Si	-46.9	1.198	0.705	-15.6	0.986	0.748	45	0	36.86

4.1. ($^{28}\text{Si}+^{90}\text{Zr}$) reaction

Figure 1. The three drawings below depict the theoretical and experimental σ_{fus} , D_{fus} and P_{fus} for the system, obtained through a combination of quantum mechanical calculations and semi-classical methods. The data used in this study are taken from Ref. [41]. The blue curves correspond to the quantum mechanical calculations with coupling and no-coupling, respectively. The blue curve with the spaces shows the results obtained with no-coupling. Similarly, the red curves, correspond to the semi-classical calculations with and no-coupling, respectively. The dashed red curve shows the results obtained no-coupling. The system's data regarding the position of the Coulomb sub-barrier V_b are sourced from the black arrow. The semi-classical calculations, no-coupling and coupling have a great concurrence with experimental data after exceeding V_b , and for below V_b , there is no concurrence with experimental data. For no-coupling and coupling quantum mechanical calculation, after exceeding V_b there is a special concurrence.

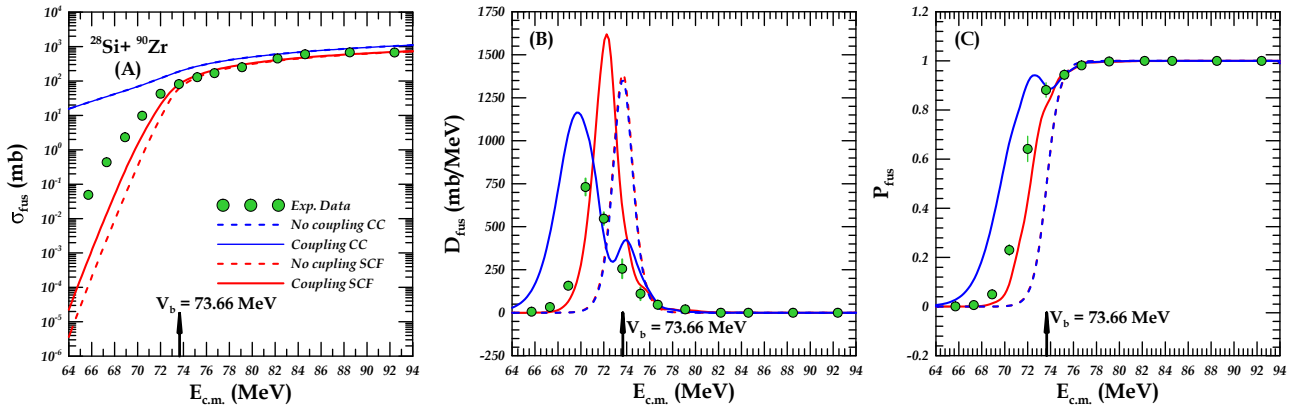


Figure 1. Displays the results of quantum mechanical and semi-classical calculations for the σ_{fus} drawing (A), D_{fus} drawing (B), and P_{fus} drawing (C), alongside experimental data [41] for the system $^{28}\text{Si}+^{90}\text{Zr}$.

4.2 ($^{28}\text{Si}+^{92}\text{Zr}$) reaction

Figure 2. The three drawings below depict the theoretical and experimental σ_{fus} , D_{fus} and P_{fus} for the system, obtained through a combination of quantum mechanical calculations and semi-classical methods. The data used in this study are taken from Ref. [42]. The blue curves correspond to the quantum mechanical calculations with coupling and no-coupling, respectively. The blue curve with the spaces shows the results obtained with no-coupling. Similarly, the red curves, correspond to the semi-classical calculations with and no-coupling, respectively. The dashed red curve shows the results obtained no-coupling. The system's data regarding the position of the Coulomb sub-barrier V_b are sourced from the black arrow. The semi-classical calculations, no-coupling and coupling have a special concurrence with experimental data after exceeding V_b and below V_b . For no-coupling and coupling quantum mechanical calculation, after exceeding V_b there is a special concurrence.

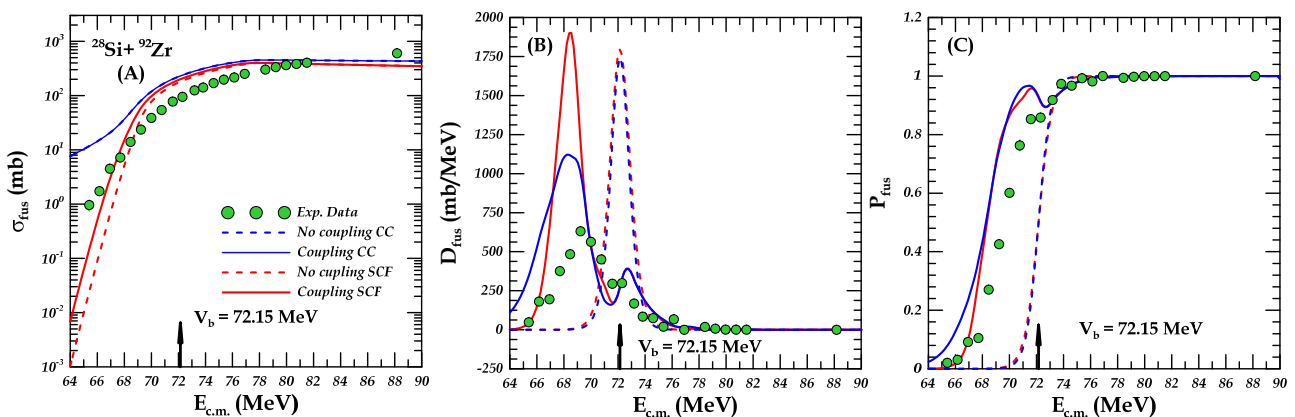


Figure 2. Displays the results of quantum mechanical and semi-classical calculations for the σ_{fus} drawing (A), D_{fus} drawing (B), and P_{fus} drawing (C), alongside experimental data [42] for the system $^{28}\text{Si}+^{92}\text{Zr}$.

4.3. ($^{28}\text{Si}+^{94}\text{Zr}$) reaction

Figure 3. The three drawings below depict the theoretical and experimental σ_{fus} , D_{fus} and P_{fus} for the system, obtained through a combination of quantum mechanical calculations and semi-classical methods. The data used in this study are taken from Ref. [41]. The blue curves correspond to the quantum mechanical calculations with coupling and no-coupling, respectively. The blue curve with the spaces shows the results obtained with no-coupling. Similarly, the red curves, correspond to the semi-classical calculations with and no-coupling, respectively. The dashed red curve shows the

results obtained no-coupling. The system's data regarding the position of the Coulomb sub-barrier V_b are sourced from the black arrow. The semi-classical calculations, no-coupling and coupling have a good concurrence with experimental data after exceeding V_b , and for below V_b , there is a special concurrence. For no-coupling and coupling quantum mechanical calculation, there is no concurrence.

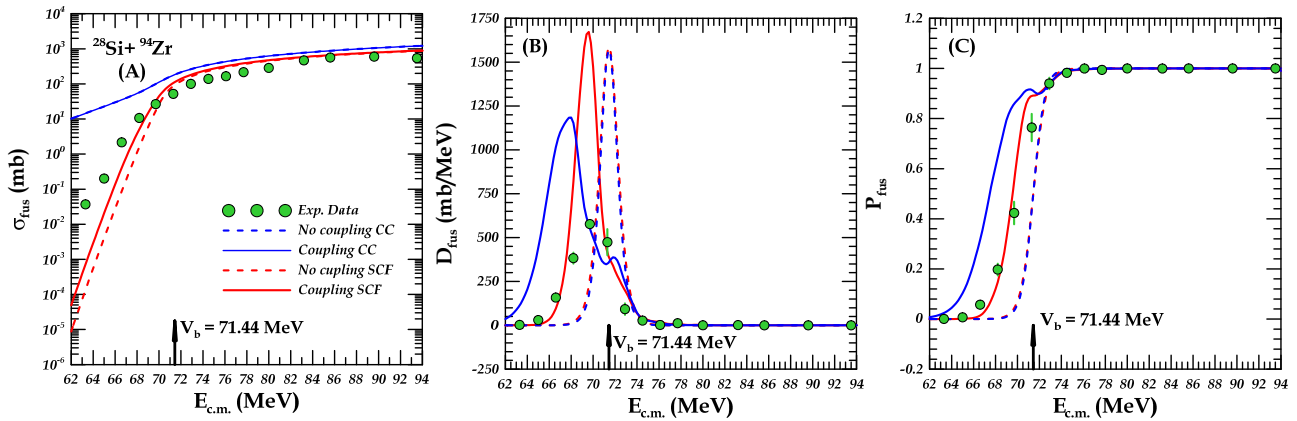


Figure 3. Displays the results of quantum mechanical and semi-classical calculations for the σ_{fus} drawing (A), D_{fus} drawing (B), and P_{fus} drawing (C), alongside experimental data [41] for the system $^{28}\text{Si}+^{94}\text{Zr}$.

4.4. ($^{41}\text{K}+^{28}\text{Si}$) reaction

Figure 4. The three drawings below depict the theoretical and experimental σ_{fus} , D_{fus} and P_{fus} for the system, obtained through a combination of quantum mechanical calculations and semi-classical methods. The data used in this study are taken from Ref. [43]. The blue curves correspond to the quantum mechanical calculations with coupling and no-coupling, respectively. The blue curve with the spaces shows the results obtained with no-coupling. Similarly, the red curves, correspond to the semi-classical calculations with and no-coupling, respectively. The dashed red curve shows the results obtained no-coupling. The system's data regarding the position of the Coulomb sub-barrier V_b are sourced from the black arrow. The semi-classical calculations, no-coupling have a special concurrence with experimental data after exceeding V_b , and for below V_b there is no concurrence, and for coupling, there is a great concurrence. For quantum mechanical calculation, there is a great concurrence after exceeding V_b .

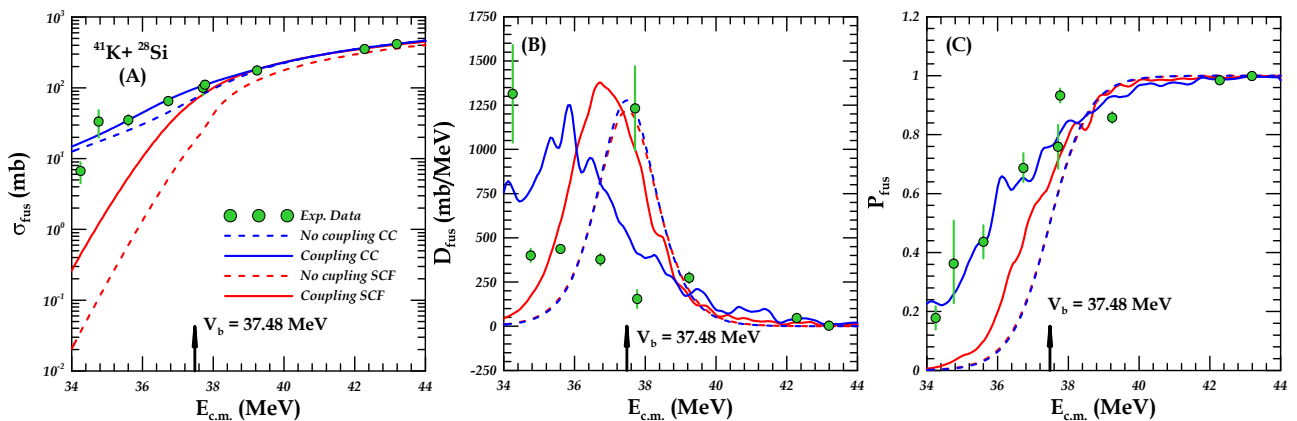


Figure 4. Displays the results of quantum mechanical and semi-classical calculations for the σ_{fus} drawing (A), D_{fus} drawing (B), and P_{fus} drawing (C), alongside experimental data [43] for the system $^{41}\text{K}+^{28}\text{Si}$.

4.5. ($^{45}\text{K}+^{28}\text{Si}$) reaction

Figure 5. The three drawings below depict the theoretical and experimental σ_{fus} , D_{fus} and P_{fus} for the system, obtained through a combination of quantum mechanical calculations and semi-classical methods. The data used in this study are taken from Ref. [43]. The blue curves correspond to the quantum mechanical calculations with coupling and no-coupling, respectively. The blue curve with the spaces shows the results obtained with no-coupling. Similarly, the red curves, correspond to the semi-classical calculations with and no-coupling, respectively. The dashed red curve shows the results obtained no-coupling. The system's data regarding the position of the Coulomb sub-barrier V_b are sourced from the black arrow. The semi-classical calculations, no-coupling and coupling have a good concurrence with experimental data after exceeding V_b . For no-coupling and coupling quantum mechanical calculation, below V_b there is a great concurrence.

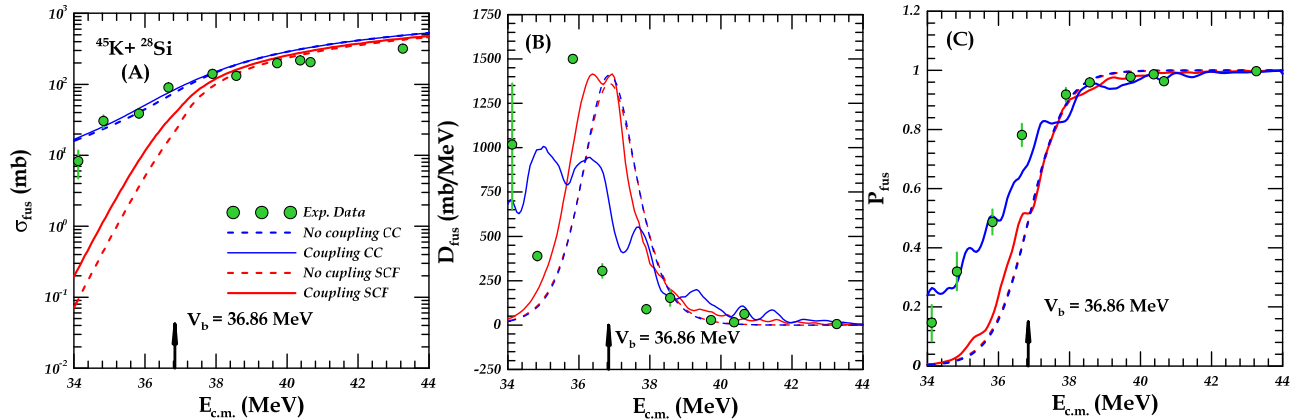


Figure 5. Displays the results of quantum mechanical and semi-classical calculations for the σ_{fus} drawing (A), D_{fus} drawing (B), and P_{fus} drawing (C), alongside experimental data [43] for the system $^{45}\text{K}+^{28}\text{Si}$.

5. CONCLUSION

The effect of channel coupling between elastic channels and breakup channels on calculating fusion cross-section (σ_{fus}), fusion barrier distribution (D_{fus}), and fusion probability (P_{fus}), on systems $^{28}\text{Si} + ^{90}\text{Zr}$, $^{28}\text{Si} + ^{92}\text{Zr}$, $^{28}\text{Si} + ^{94}\text{Zr}$, $^{41}\text{K} + ^{28}\text{Si}$, and $^{45}\text{K} + ^{28}\text{Si}$ were investigated in the present study and these systems involved one neutron or one proton transfer reactions. Our theoretical calculations showed that the results improved significantly below the Coulomb barrier, especially the semi-classical calculations. The reason for the improvement below the Coulomb barrier can be attributed to the fact that coupling effects become more significant at lower energies, leading to a more complex interaction between the elastic channels and the breakup channels. Introducing coupling conditions into the calculations takes into account the exchange of flow between these channels, which results in better agreement with the experimental data. On the other hand, the slight overestimation of the results above the Coulomb barrier can be attributed to the fact that the fusion process becomes more controlled by the elastic channel at higher energies, and the coupling effects become less significant. The reason for the overestimation of the cross-section may be the fact that our calculations may not have fully accounted for the effect of the Coulomb barrier on the merger process.

ORCID

✉ M.A. Khuadher, <https://orcid.org/0009-0006-5372-547X>; ✉ F.A. Majeed, <https://orcid.org/0000-0002-0701-9084>

REFERENCES

- [1] M. Beckerman, "Sub-barrier fusion of two nuclei," Reports on Progress in Physics, **51**(8), 1047 (1988). <https://doi.org/10.1088/0034-4885/51/8/001>
- [2] J.E. Johnstone, V. Singh, R. Giri, S. Hudan, J. Vadas, R.T. Desouza, D. Ackermann, A. Chbihi, Q. Hourdille, A. Abbott, and C. Balhoff, "Proton and neutron exchange as a prelude to fusion at near-barrier energies," Physical Review C, **106**(1), L011603, (2022). <https://doi.org/10.1103/PhysRevC.106.L011603>
- [3] K. Hammerton, Z. Kohley, D.J. Hinde, M. Dasgupta, A. Wakhle, E. Williams, V.E. Oberacker, A.S. Umar, I.P. Carter, K.J. Cook, and J. Greene, "Reduced quasifission competition in fusion reactions forming neutron-rich heavy elements," Physical Review C, **91**(4), 041602 (2015). <https://doi.org/10.1103/PhysRevC.91.041602>
- [4] S. Hudan, R.T. deSouza, A.S. Umar, Z. Lin, and C.J. Horowitz, "Enhanced dynamics in fusion of neutron-rich oxygen nuclei at above-barrier energies," Physical Review C, **101**(6), 061601 (2020). <https://doi.org/10.1103/PhysRevC.101.061601>
- [5] H.M. Jia, C.J. Lin, L. Yang, X.X. Xu, N.R. Ma, L.J. Sun, F. Yang, Z.D. Wu, H.Q. Zhang, Z.H. Liu, and D.X. Wang, "A self-consistent method to analyze the effects of the positive Q-value neutron transfers on fusion," Physics Letters B, **755**, 43-46 (2016). <https://doi.org/10.1016/j.physletb.2016.01.058>
- [6] M. Beckerman, M. Salomaa, A. Sperduto, H. Enge, J. Ball, A. DiRienzo, S. Gazes, Y. Chen, J.D. Molitoris, and M. Nai-Feng, "Dynamic influence of valence neutrons upon the complete fusion of massive nuclei," Physical Review Letters, **45**(18), 1472 (1980). <https://doi.org/10.1103/PhysRevLett.45.1472>
- [7] R.A. Broglia, C.H. Dasso, S. Landowne, and A. Winther, "Possible effect of transfer reactions on heavy ion fusion at sub-barrier energies," Physical Review C, **27**(5), 2433 (1983). <https://doi.org/10.1103/PhysRevC.27.2433>
- [8] S. Kalkal, S. Mandal, N. Madhavan, E. Prasad, S. Verma, A. Jhingan, R. Sandal, S. Nath, J. Gehlot, B.R. Behera, and M. Saxena, "Channel coupling effects on the fusion excitation functions for $\text{Si}^{28} + \text{Zr}^{90,94}$ in sub- and near-barrier regions," Physical Review C, **81**(4), 044610 (2010). <https://doi.org/10.1103/PhysRevC.81.044610>
- [9] A.M. Stefanini, L. Corradi, A.M. Vinodkumar, Y. Feng, F. Scarlassara, G. Montagnoli, S. Beghini, and M. Bisogno, "Near-barrier fusion of $^{36}\text{S} + ^{90,96}\text{Zr}$: The effect of the strong octupole vibration of ^{96}Zr ," Physical Review C, **62**(1), 014601 (2000). <https://doi.org/10.1103/PhysRevC.62.014601>
- [10] V.Y. Denisov, "Subbarrier heavy ion fusion enhanced by nucleon transfer," The European Physical Journal A-Hadrons and Nuclei, **7**, 87-99 (2000). <https://doi.org/10.1007/s100500050015>
- [11] W. Kohn, and L.J. Sham, "Self-consistent equations including exchange and correlation effects," Physical Review, **140**, A1133 (1965). <https://doi.org/10.1103/PhysRev.140.A1133>

- [12] V. Singh, J. Vadas, T. K. Steinbach, B. B. Wiggins, S. Hudan, R. T. deSouza, Z. Lin, C. J. Horowitz, L. T. Baby, S. A. Kuvin, and V. Tripathi, "Fusion enhancement at near and sub-barrier energies in $^{19}\text{O}+^{12}\text{C}$," *Phys. Lett. B*, **765**, 99 (2017). <https://doi.org/10.1016/j.physletb.2016.12.017>
- [13] B.A. Bian, F.S. Zhang, and H.Y. Zhou, "Fusion enhancement in the reactions of neutron-rich nuclei," *Nucl. Phys. A*, **829**, 1 (2009). <https://doi.org/10.1016/j.nuclphysa.2009.08.003>
- [14] C. Beck, "Transfer/Breakup Channel Couplings in Sub-barrier Fusion Reactions," *J. Phys. Conf. Ser.* **420**, 012067 (2013). <https://doi.org/10.1088/1742-6596/420/1/012067>
- [15] N. Rowley, I.J. Thompson, and M.A. Nagarajan, "Neutron flow and necking in heavy-ion fusion reactions," *Phys. Lett. B*, **282**, 276 (1992). [https://doi.org/10.1016/0370-2693\(92\)90638-K](https://doi.org/10.1016/0370-2693(92)90638-K)
- [16] R. Pengo, D. Evers, K.E.G. Löbner, U. Quade, K. Rudolph, S.J. Skorka, and I. Weidl, "Nuclear structure effects in sub-barrier fusion cross sections," *Nucl. Phys. A*, **411**, 255 (1983). [https://doi.org/10.1016/0375-9474\(83\)90392-5](https://doi.org/10.1016/0375-9474(83)90392-5)
- [17] H. Timmers, D. Ackermann, S. Beghini, L. Corradi, J.H. He, G. Montagnoli, F. Scarlassara, A.M. Stefanini, and N. Rowley, "A case study of collectivity, transfer and fusion enhancement," *Nucl. Phys. A*, **633**, 421 (1998). [https://doi.org/10.1016/S0375-9474\(98\)00121-3](https://doi.org/10.1016/S0375-9474(98)00121-3)
- [18] V.I. Zagrebaev, "Sub-barrier fusion enhancement due to neutron transfer," *Phys. Rev. C*, **67**, 061601(R) (2003). <https://doi.org/10.1103/PhysRevC.67.061601>
- [19] M.S. Gautam, S. Duhan, R.P. Chahal, H. Khatri, S.B. Kuhar, and K. Vinod, "Influence of neutron transfer channels and collective excitations in the fusion of Si^{28} with $\text{Zr}^{90,92,94,96}$ targets," *Phys. Rev. C*, **102**, 014614 (2020). <https://doi.org/10.1103/PhysRevC.102.014614>
- [20] G.L. Zhang, X.X. Liu, and C.J. Lin, "Systematic analysis of the effect of a positive Q-value neutron transfer in fusion reactions," *Phys. Rev. C*, **89**, 054602 (2014). <https://doi.org/10.1103/PhysRevC.89.054602>
- [21] F.A. Majeed, Y.A. Abdul-Hussien, and F.M. Hussian, "Fusion Reaction of Weakly Bound Nuclei," in: *Nuclear Fusion-One Noble Goal and a Variety of Scientific and Technological Challenges*, edited by I. Girka, (University of Kharkiv, Ukraine, 2019). <https://doi.org/10.5772/intechopen.80582>
- [22] F.K. Ahmed, F.A. Majeed, and T.M. Abbass, *The Effect of Breakup on the Total Fusion Reaction Cross Section of Stable Bound Nuclei*, (University of Babylon, 2012). <https://repository.uobabylon.edu.iq/papers/publication.aspx?Pubid=5446>
- [23] F.A. Majeed, and Y.A. Abdul-Hussien, "Fusion and Breakup Reactions of $^{17}\text{S}+^{208}\text{Pb}$ and $^{15}\text{C}+^{232}\text{Th}$ Halo Nuclei Systems," *J. Adv. Phys.* **11**, 2 (2015). <https://rajpub.com/index.php/jap/article/view/495jap>
- [24] F.A. Majeed, and Y.A. Abdul-Hussien, "Semiclassical treatment of fusion and breakup processes of $^{6,8}\text{He}$ halo nuclei," *J. Theor. Appl. Phys.* **10**(2), 107-112 (2016). <https://doi.org/10.1007/s40094-016-0207-y>
- [25] L.F. Canto, R. Donangelo, and H.D. Marta, "Semiclassical treatment of fusion processes in collisions of weakly bound nuclei," *Phys. Rev. C*, **73**, 034608 (2006). <https://doi.org/10.1103/PhysRevC.73.034608>
- [26] K. Alder, and A. Winther, *Electromagnetic Excitations*, (North-Holland, Amsterdam, 1975)
- [27] P.R.S. Gomes et al., "Effect of the breakup on the fusion and elastic scattering of weakly bound projectiles on $\text{Zn } 64$," *Phys. Rev. C*, **71**, 034608 (2005). <https://doi.org/10.1103/PhysRevC.71.034608>
- [28] L. F. Canto et al., "Recent developments in fusion and direct reactions with weakly bound nuclei," *Phys. Rep.* **596**, 1-86 (2015). <https://doi.org/10.1016/j.physrep.2015.08.001>
- [29] C.A. Bertulani, and L.F. Canto, "Semiclassical calculation of Coulomb break-up of weakly-bound nuclei," *Nucl. Phys. A*, **539**, 163-176 (1992). [https://doi.org/10.1016/0375-9474\(92\)90240-K](https://doi.org/10.1016/0375-9474(92)90240-K)
- [30] P. Gomes, T. Penna, R.L. Neto, J. Acquadro, C. Tenreiro, P. Freitas, E. Crema, NC Filho, and M. Coimbra, "Nuclear fusion between heavy ions by the gamma-ray spectroscopy method," *Nucl. Instr. and Meth. A*, **280**, 395 (1989). [https://doi.org/10.1016/0168-9002\(89\)90940-6](https://doi.org/10.1016/0168-9002(89)90940-6)
- [31] M.S. Hussein, M.P. Pato, L.F. Canto, and R. Donangelo, "Real part of the polarization potential for induced 11 fusion reactions," *Physical Review C*, **47**(5), 2398-2402 (1993). <https://doi.org/10.1103/PhysRevC.47.2398>
- [32] J.F. Liang, and C. Signorini, "Fusion induced by radioactive ion beams," *International Journal of Modern Physics E*, **14**(8), 1121-1150 (2005). <https://doi.org/10.1142/S021830130500382X>
- [33] K. Alder, and A. Winther, *Electromagnetic Excitations*, (North-Holland, Amsterdam, 1975).
- [34] M. Abramowitz, and I.A. Stegun, *Handbook of Mathematical Functions*, (Dover Publications, New York, 1964).
- [35] P.R.S. Gomes, J. Lubian, I. Padron, R.M. Anjos, D.R. Otomar, L.C. Chamon, and E. Crema, "Fusion, break-up and scattering bound nuclei," *Revista Mexicana de Física*, **52**, 23-29 (2006). https://www.scielo.org.mx/scielo.php?pid=S0035-001X2006001000006&script=sci_abstract&tlng=pt
- [36] L.F. Canto, R. Donangelo, and H.D. Marta, "Upper bounds for fusion processes in collisions of weakly bound nuclei," *Brazilian Journal of Physics*, **35**, 884-887 (2005). <https://doi.org/10.1590/S0103-97332005000500045>
- [37] M. Abramowitz, and I.A. Stegun, *Handbook of Mathematical Functions*, National Bureau of Standards, Applied Mathematics Series, vol. 55 (1972).
- [38] N. Rowley, G.R. Satchler, and P.H. Stelson, "On the 'distribution of barriers' interpretation of heavy-ion fusion," *Physics Letters B*, **254**(1-2), 25-29 (1991). [https://doi.org/10.1016/0370-2693\(91\)90389-8](https://doi.org/10.1016/0370-2693(91)90389-8)
- [39] F.M. Nunes, and I.J. Thompson, "Multistep effects in sub-Coulomb breakup," *Physical Review C*, **59**(5), 2652 (1999). <https://doi.org/10.1103/PhysRevC.59.2652>
- [40] L.F. Canto, R. Donangelo, and H.D. Marta, "Semiclassical treatment of fusion processes in collisions of weakly bound nuclei," *Physical Review C*, **73**, 034608 (2006). <https://doi.org/10.1103/physrevc.73.034608>
- [41] S. Kalkal, S. Mandal, N. Madhavan, E. Prasad, S. Verma, A. Jhingan, R. Sandal, S. Nath, J. Gehlot, B.R. Behera, and M. Saxena, "Channel coupling effects on the fusion excitation functions for $\text{Si}^{28}+\text{Zr}^{90,94}$ in sub- and near-barrier regions," *Physical Review C*, **81**(4), 044610 (2010). <https://doi.org/10.1103/PhysRevC.81.044610>
- [42] J.O. Newton, C.R. Morton, M. Dasgupta, J.R. Leigh, J.C. Mein, D.J. Hinde, H. Timmers, and K. Hagino, "Experimental barrier distributions for the fusion of ^{12}C , ^{16}O , ^{28}Si , and ^{35}Cl with ^{92}Zr and coupled-channels analyses," *Physical Review C*, **64**(6), 064608 (2001). <https://doi.org/10.1103/PhysRevC.64.064608>

[43] J.E. Johnstone, PhD thesis, “The influence of shell structure on near-barrier fusion of neutron-rich nuclei”, Indiana University, 2022.

**ВПЛИВ ПРОТОНА І НЕЙТРОНА ЯК ЗОНДА ДЛЯ РЕАКЦІЇ ЯДЕРНОГО СИНТЕЗУ
ПРИ НАВКОЛОБАР'ЄРНИХ ЕНЕРГІЯХ**

М.А. Хуадер, Ф.А. Маджид

Факультет фізики, Освітній коледж чистих наук, Вавилонський університет, Ірак

У цьому дослідженні квантово-механічні розрахунки та напівкласичний підхід використовувалися для визначення ймовірності термоядерного синтезу (P_{fus}), розподілу бар'єрів термоядерного синтезу (D_{fus}) і поперечного перерізу синтезу (σ_{fus}) для систем $^{28}\text{Si} + ^{90}\text{Zr}$, $^{28}\text{Si} + ^{92}\text{Zr}$, $^{28}\text{Si} + ^{94}\text{Zr}$, $^{41}\text{K} + ^{28}\text{Si}$, and $^{45}\text{K} + ^{28}\text{Si}$. Напівкласичний підхід передбачав використання наближення Венцеля–Крамерса–Бріллюена (WKB) для опису відносного руху між снарядом і цільовими ядрами та методу дискретизованого пов'язаного каналу (CDCC) Альдера–Вінтера (AW) для опису власний рух ядер. Результати показали, що врахування розрахунків каналу зв'язку для квантової механіки та напівкласичного підходу та його впливу на P_{fus} , D_{fus} та σ_{fus} для досліджуваних систем, що включають реакції переносу одного нейтрона або одного протона, є дуже важливим для розгляду зокрема навколо та під кулонівським бар'єром. Результати порівнювали з даними вимірювань і виявили розумну збіг.

Ключові слова: *канал розпаду; пружний канал; ядерний синтез; перенесення нейтронів; перенесення протонів*